Annales Geophysicae (2001) 19: 327–339 © European Geophysical Society 2001

Annales Geophysicae

A case study of HF radar spectra and 630.0 nm auroral emission in the pre-midnight sector

M. Lester[1], **S. E. Milan**[1], **V. Besser**[2], **and R. Smith**[2]

[1]Department of Physics and Astronomy, University of Leicester, Leicester, LE1 7RH, United Kingdom
[2]Geophysical Institute, University of Alaska, Fairbanks, Alaska, U.S.A.

Received: 19 September 2000 – Revised: 19 February 2001 – Accepted: 20 February 2001

Abstract. A comparison of HF radar backscatter observed by the CUTLASS Finland radar, meridian scanning photometer data from Longyearbyen, magnetic field variations from IMAGE stations, and particle precipitation measured by the DMSP F12 spacecraft is presented. The interval under discussion occurred in the pre-midnight local time sector, during a period of weakly northward interplanetary magnetic field. A region of HF backscatter, typically 8 degrees wide, occurred in the field of view of the CUTLASS Finland radar. A well defined gradient in the spectral width parameter was present, with mainly low (< 200 m s^{-1}) spectral widths in the lower latitude part of the scatter and predominantly large (> 200 ms^{-1}) spectral widths in the higher latitude part. The relationship between the spectral width and the red line (630.0 nm) emission measured by the meridian scanning photometer is considered. The poleward border of the red line emission, which has, in the past, been proposed as being representative of the polar cap boundary, was colocated to within 1° of magnetic latitude with the gradient in spectral width for part of the interval. Statistically, large spectral widths occurred poleward of the red line emission, while small spectral widths occurred within or equatorward of the red line emission. Near simultaneous DMSP particle observations in the 20 eV to 20 keV range indicate that the poleward border of the red line emission and the gradient in spectral width occurred at the same latitude as the transition from auroral oval to polar rain particle energies. We conclude that the large spectral widths were not caused by particle precipitation associated with the auroral oval. There were two periods of special interest when the relationship between the red line and the spectral width broke down. The first of these happened during enhanced red line and green line (557.7 nm) emission, with a drop out of the radar scatter and an enhanced, narrow westward electrojet. We conclude that this event was a magnetospheric substorm occurring at much higher than usual latitudes. The second period of special interest happened when equatorward moving bands of large spectral width occurred within the region of scatter. Up to 4 of these bands were present during an interval of 100 minutes. Associated with these narrow bands of large spectral width were narrow channels of enhanced westward ion velocities. We conclude that these equatorward moving bands of large spectral width may be related to reconnection processes in the tail. The observations demonstrate that the tail continues to be active even under low solar wind energy input conditions. Furthermore, we conclude that the gradient in the spectral width may be used as a proxy for the polar cap boundary, but only with extreme caution.

Key words. Ionosphere (ionosphere-magnetosphere interactions; polar ionosphere) – Magnetospheric physics (storms and substorms)

1 Introduction

The boundary between open and closed magnetic field lines, when mapped into the ionosphere, is often termed the polar cap boundary. The motion of this boundary, and hence, the size of the polar cap and the amount of open flux in the magnetosphere, in response to solar wind, interplanetary magnetic field (IMF) conditions, and magnetospheric substorms is a topic of considerable interest. Magnetic reconnection at the dayside magnetopause and in the tail creates and destroys the open magnetic flux and, in so doing, drives a convection cycle in the magnetosphere which maps into the ionosphere (see e.g. Cowley, 1998, for a review). It is well established (e.g. Reiff and Burch, 1985; Cowley, 1998) that the ionospheric convection pattern is controlled by the direction of the IMF. The average convection pattern during IMF B_z negative conditions consists of two cells with antisunward flow across the polar cap and sunward flow at lower latitudes. The IMF B_y component distorts the two cells such that the dusk cell (dawn cell) is dominant for positive (negative) B_y. In addition to reconnection, there is evidence of a viscous interaction which drives flows in the same direction as those

Correspondence to: M. Lester (mle@ion.le.ac.uk)

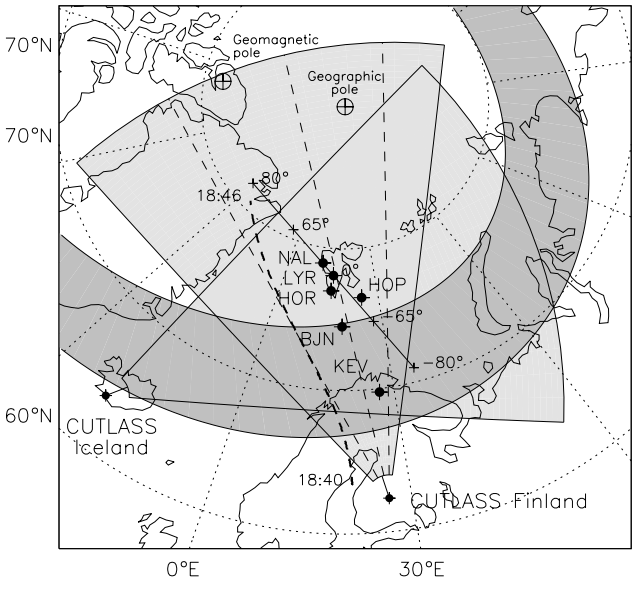

Fig. 1. Map showing the fields of view of the CUTLASS radars at Hankasalmi, Finland and Pykkvibaer, Iceland. The directions of three of the 16 beams, 4 (eastern), 9 (central) and 13 (western), of the Finland radar are marked by dashed lines. The direction of the scan of the meridian scanning photometers at Longyearbyen (full line), the locations of five IMAGE magnetometer stations (crosses), and the trajectory of the DMSP spacecraft, F12, (thick dashed line) are also shown.

driven by reconnection, albeit at much weaker levels. This is particularly clear when the IMF has a northward component. However, during northward IMF, it is also possible for reconnection between the IMF and the tail lobes to take place for particularly favourable orientations of IMF B_y and B_x. This produces the so-called lobe cells at higher latitudes, where the reconnection site is located poleward of the viscous cells. The effect of the viscous interaction during southward IMF B_z is to move the centre of the two flow cells to lower latitudes, thereby displacing the flow reversal boundary (FRB) from the boundary between open and closed magnetic flux, i.e. the polar cap boundary (PCB).

The impact of magnetospheric substorms on ionospheric convection is less understood. It is generally accepted that open flux in the tail will be reconnected during the substorm process, although no quantitative estimate of the percentage of the existing open flux that is reconnected has yet been made. Furthermore, as reconnection at the dayside magnetopause is responsible for ionospheric convection on the dayside, it might be expected that reconnection in the tail should also drive convection. However, although the current systems during magnetospheric substorms are well known (e.g. Kamide and Kokubun, 1996), the ionospheric flows are less understood, in particular during the expansion and recovery phases (e.g. Lester, 2000). It is clear, however, that substorms do result in the contraction of the polar cap boundary (e.g. Lockwood et al., 1988; Lester et al., 1990; Taylor et al., 1996), which does indicate that open magnetic flux is destroyed during the substorm process.

To gain a quantitative understanding of how the open magnetic flux in the magnetosphere varies as a function of the IMF and substorm activity, it is necessary to be able to follow the location of the PCB at all local times. Currently, there is no unambiguous method of doing this. There are many ways to locate the FRB using networks of ground-based radars such as SuperDARN (Greenwald et al., 1995) or networks of magnetometers using the AMIE technique (e.g. Taylor et al., 1996). However, the FRB and the PCB may not necessarily be co-located, as mentioned above. The particle distributions measured by low earth orbiting spacecraft, such as DMSP and FAST, can also be used to identify the boundary between auroral precipitation and polar rain. This represents one diagnostic for the PCB (e.g. Newell et al., 1996). There are not sufficient spacecraft, however, to provide true global coverage with sufficient temporal resolution. Global images of the UV aurora can also be used (e.g. Brittnacher et al., 1999), but these too do not always identify the PCB clearly. Networks of meridian scanning photometers could also be used since the poleward border of the 630.0 nm (red line) auroral emission may be located with the PCB (e.g. Samson et al., 1992; Blanchard et al., 1995). Such a technique, however, will only work in darkness.

In this paper we investigate the relationship between the red line emission and the spectral width parameter of HF radar backscatter, as measured by the CUTLASS Finland radar. A particular feature in the spectral width is the existence of large spectral width values at the poleward side of a region of scatter, resulting in a latitudinal gradient in the spectral width. The purpose is to address the cause of the large spectral width values and hence, the gradient in order to identify potential magnetospheric boundaries associated with this gradient, and to judge whether this feature may be used in future as a diagnostic of the PCB. In addition, the interval of interest contains two dynamic features of interest: a weak substorm expansion occurring at high magnetic latitudes, and equatorward moving bands of high spectral width after this substorm. These dynamic features will also be discussed.

2 Experimental overview

CUTLASS consists of two HF radars, one of which is located at Hankasalmi, Finland and the other at Pykkvibaer, Iceland (Lester et al., 1997). The fields of view overlap from northern Norway to poleward of Svalbard (see Fig. 1). The two radars form the eastern most pair of the northern hemisphere chain of SuperDARN radars (Greenwald et al., 1995). Each radar provides measurements of three basic parameters: the backscatter power, the line of sight velocity, and the spectral width, in 75 range gates along each of 16 look directions. In their normal mode of operation, the SuperDARN HF radars integrate for 7 s along each beam direction and scan 16 beam directions successively such that a full scan takes 2 minutes. The line of sight velocities from the overlapping part of the

fields of view of the two radars can be combined to form vector velocities in the ionosphere. Alternatively, the line of sight velocity measurements from all radars can be combined to create maps of the ionospheric potential (Ruohoniemi and Baker, 1998). In this paper, however, we concentrate solely on data from the Finland radar.

At Longyearbyen, a meridian scanning photometer operates at four different wavelengths: 427.8 nm, 486.1 nm, 557.7 nm and 630.0 nm. In the following analysis we concentrate on the 630.0 nm (red line) and 557.7 nm (green line) wavelengths. The photometer scans from 0° elevation in the north to 0° elevation in the south in a time interval of 2 seconds, with a repeat cycle of 16 seconds. The scan direction of the photometer is oriented at an azimuth of 45 degrees to geographic north (Fig. 1). Also shown in Fig. 1 are the directions of beams 4, 9 and 13 of the CUTLASS Finland radar, as well as the locations of five of the IMAGE magnetometer stations (Viljanen and Häkkinen, 1997) from Ny Alesund (NAL) to Kevo (KEV), which have also been used in this study. A DMSP overpass is employed to determine the locations of boundaries in the precipitation and the trajectory of this overpass is indicated in Fig. 1.

3 Observations

The interval of interest is 1850–2300 UT on 27 November 1997. In the top three panels of Fig. 2 we present the IMF conditions as measured by the Magnetic Field Instrument, MFI, (Lepping et al., 1995) on the WIND spacecraft which was located at (191, −8, 28) R_E (GSM X, Y and Z coordinates). The interval presented in Fig. 2 extends from 1700–2200 UT. Comparison with IMP-8 data (not shown), which was located at (6.2, −27.4, −22.9) R_E (GSM coordinates), demonstrates that the IMF measured by the two spacecraft at these two different locations is, in general, very similar. This indicates that the measurements by WIND were representative of the conditions which impinged on the magnetosphere. Also, based upon this comparison, it is estimated that the delay between the measurement at WIND and the impact of the IMF at the dayside magnetopause was approximately one hour. Thus, the time interval presented in Fig. 2 is effectively 1800–2300 UT at the dayside magnetopause and the times quoted below will, from hereon, be the approximate times at the magnetopause. The IMF B_x component was about +2 nT at the start of the interval and gradually changed to about −4 nT at the end, changing sign at ∼1912 UT. The B_y component remained negative throughout the interval, varying between −1 nT and −6 nT. Finally, the IMF B_z component began at ∼−4 nT before becoming weakly positive at ∼1824 UT and remained so until ∼2136 UT when it became +4 nT. During much of the interval of weakly positive B_z, the B_y component was of the order of twice the B_z component. The solar wind velocity (Fig. 2, panel 4) measured by the Solar Wind Experiment, SWE, (Ogilvie et al., 1995) began at about 340 km s^{-1} and gradually increased to about 360 km s^{-1} over the interval. The solar wind density (Fig. 2, bottom panel), also measured by SWE, varied between 4 cm^{-3} and 6 cm^3.

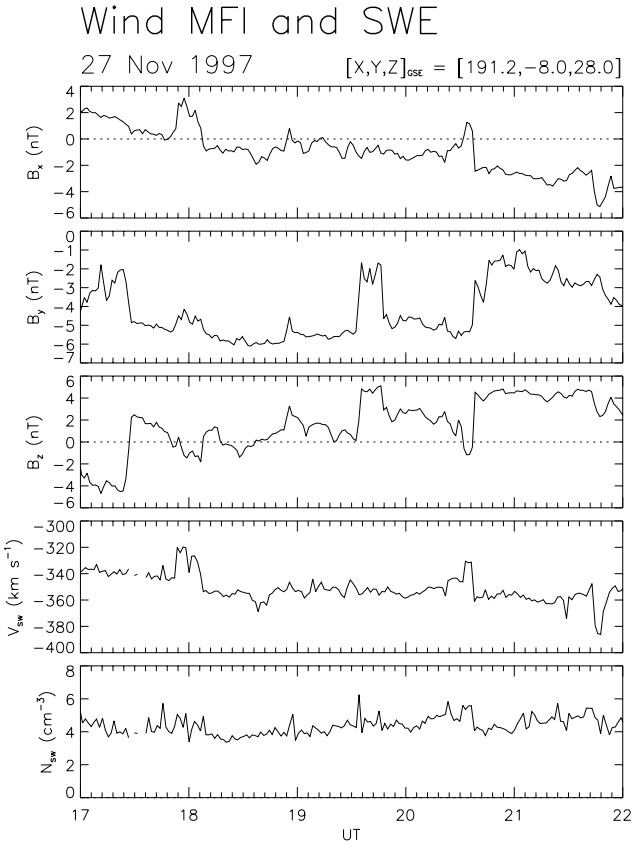

Fig. 2. Wind measurements of the IMF and solar wind velocity and density for the interval 17–22 UT on 27 November 1997.

Before moving to the radar and optical observations, we present the magnetometer data from the northernmost stations of the IMAGE array in Fig. 3a (X component) and Fig. 3b (Z component). The locations of the stations relative to the radar field of view and the MSP meridian are given in Fig. 1. We only present these stations as the stations at lower latitudes show small variations which are not dissimilar from those at KEV. There was a clear negative excursion of the X (north-south) component at 1917 UT (dashed vertical line), which maximised at HOP where the deflection was of order 120 nT. Weaker negative excursions in the X component also occurred at LYR, HOR and BJN. There is evidence of some form of recovery at ∼1932 UT, although another negative excursion was then seen at 1939 UT (dashed vertical line). At 1955 UT (dashed vertical line), the X component at all stations appeared to have recovered to the levels observed before 1917 UT, where, at such time, the Z (vertical) component had positive deflections at NAL, LYR and HOR, while at HOP, the deflection was initially positive before oscillating quite strongly between positive and negative. At BJN, the initial deflection was negative at 1917 UT. These observations are consistent with an enhanced westward electrojet which is centred near HOR (73.9° magnetic latitude)

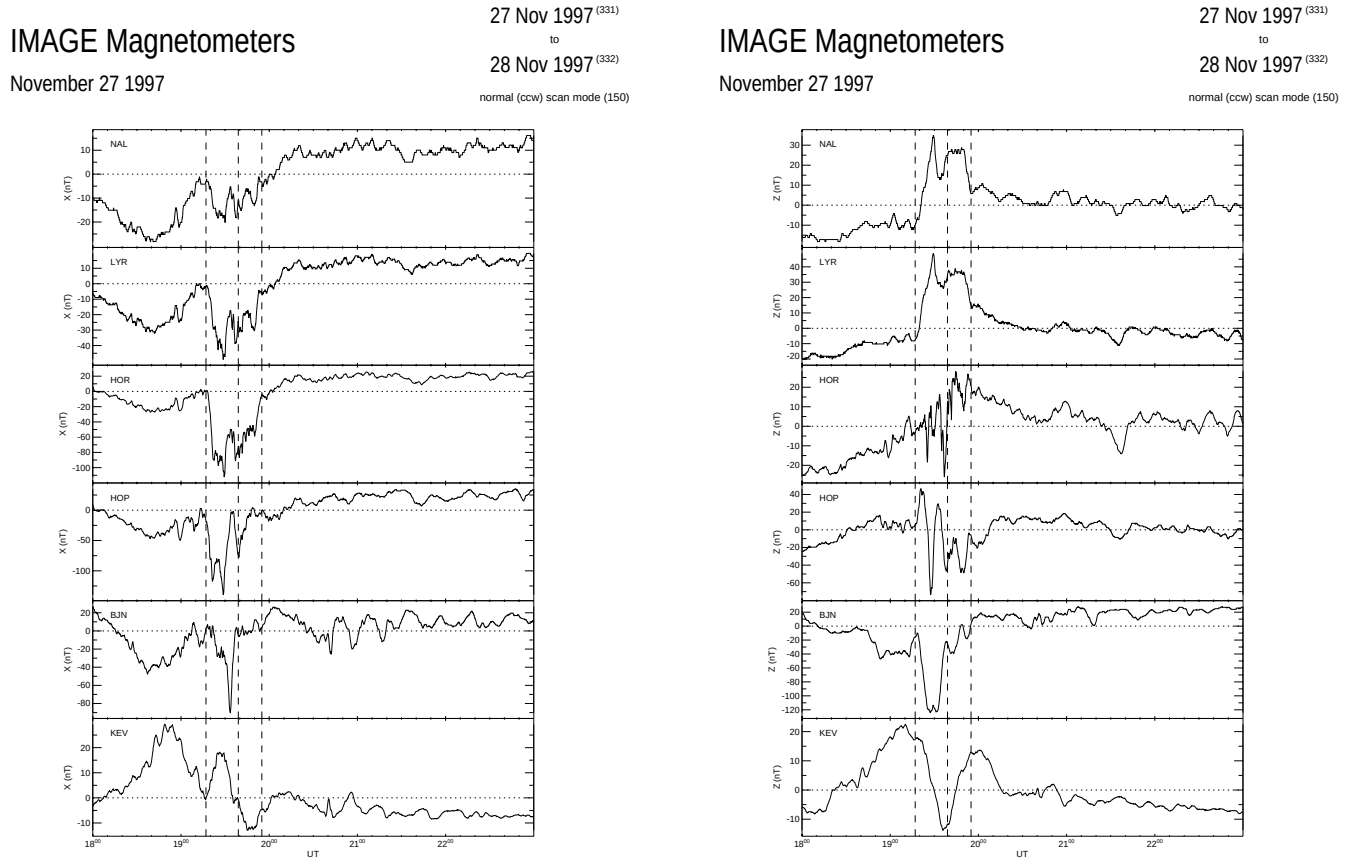

Fig. 3. (a) *X* (north-south) and **(b)** *Z* (vertical) magnetograms from the 5 IMAGE stations shown in Fig. 1 for the interval 18–23 UT on 27 November 1997. The dashed vertical lines identify times of interest.

and extends to BJN (71.2° magnetic latitude) in the south and at least NAL (76° magnetic latitude) in the north. This is a fairly weak electrojet when compared with electrojets observed during typical substorm expansion phases on the IMAGE array (e.g. Lester et al., 1995; Fox et al., 1999). We return to this magnetic activity later in the discussion.

In Fig. 4 we present the observations along beam 9 of CUTLASS Finland of the three main radar parameters: backscatter power, line of sight velocity and spectral width (top three panels) as a function of magnetic latitude and UT. The interval 1800–2300 UT is equivalent to ∼2000–0100 MLT for this beam. The intensity of the 630.0 and 557.7 nm emissions from the Longyearbyen MSP are plotted in Fig. 4's bottom two panels, as a function of zenith angle and UT. The radar data have been taken from beam 9 since this beam passes over Longyearbyen at 74.9° magnetic latitude. The top three panels indicate that radar backscatter first appeared just before 1850 UT and was present for most of the remainder of the interval, apart from a short period between 1912 and 1920 UT, which we will discuss later. The backscatter initially extended over the region 68–76° magnetic latitude, although this latitudinal extent was reduced by the end of the interval. The line of sight velocities were, in general, small and positive (towards the radar), apart from three intervals, which start at 1930, 1942 and 1950 UT, when there are larger positive velocities at the poleward limit of the backscatter. In the spectral width measurements (Fig. 4, panel 3), there was a well defined boundary between small spectral widths in the equatorward part of the backscatter and larger spectral widths in the poleward part of the backscatter. This boundary between the two types started at about 72° magnetic latitude, when the backscatter was first observed at 1850 UT, and moved gradually poleward until the loss of backscatter occurred on beam 9 on the scan, starting at 1914 UT. When the scatter returned, large spectral widths existed at almost all latitudes until about 1935 UT, when the boundary was re-established near 71° magnetic latitude. Thereafter, there was a poleward motion to 72° magnetic latitude until about 1945 UT. This boundary remained at that latitude until about 2005 UT, when it began to move equatorward, eventually reaching 69.5° magnetic latitude just before 2040 UT. There followed a number of bands of large spectral width which moved equatorward at approximately similar rates, i.e. ∼2° of magnetic latitude in 20 minutes, equivalent to ∼200 m s^{-1}. On beam 9, there were three clear examples of these bands, starting at the approximate times of 2020 UT, 2110 UT and 2135 UT, with a further possible event at 2045 UT. The minimum magnetic latitude to which these bands propagated was 69.5°. After 2200 UT, the boundary remained near 70° magnetic latitude until about 2240 UT, when it started to move poleward again,

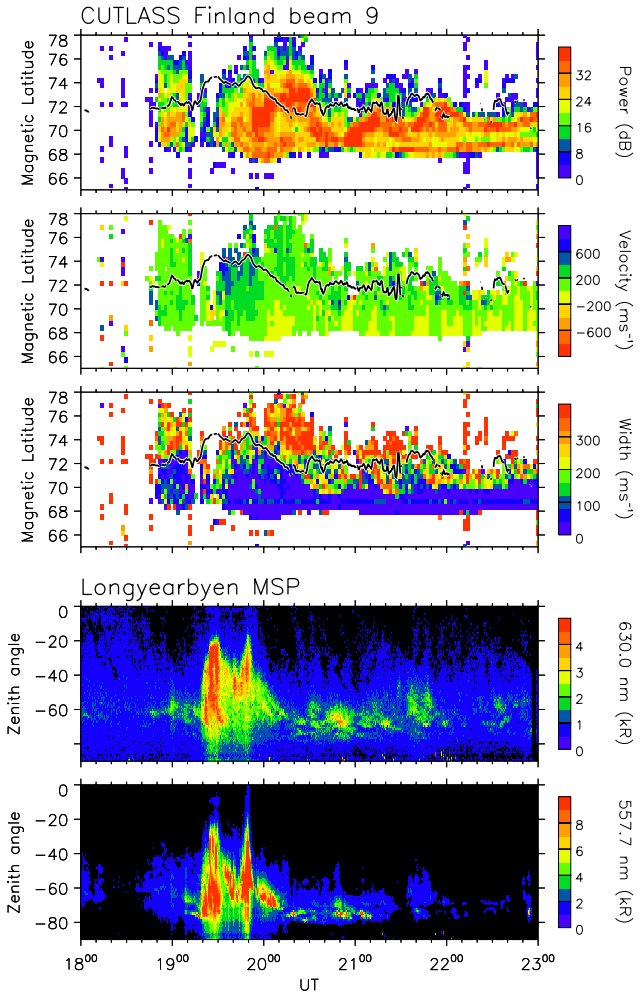

Fig. 4. Backscatter power, line of sight velocity and spectral width from beam 9 of CUTLASS Finland, as a function of latitude for the interval 18–23 UT on 27 November 1997. Also plotted are the 630.0 nm emission intensity and the 557.7 nm emission intensity as a function of zenith angle from 0° to −90° for the same interval. The full line marked on each panel of the radar data represents the poleward 1.5 kR contour of the 630.0 nm emission (see text for full discussion).

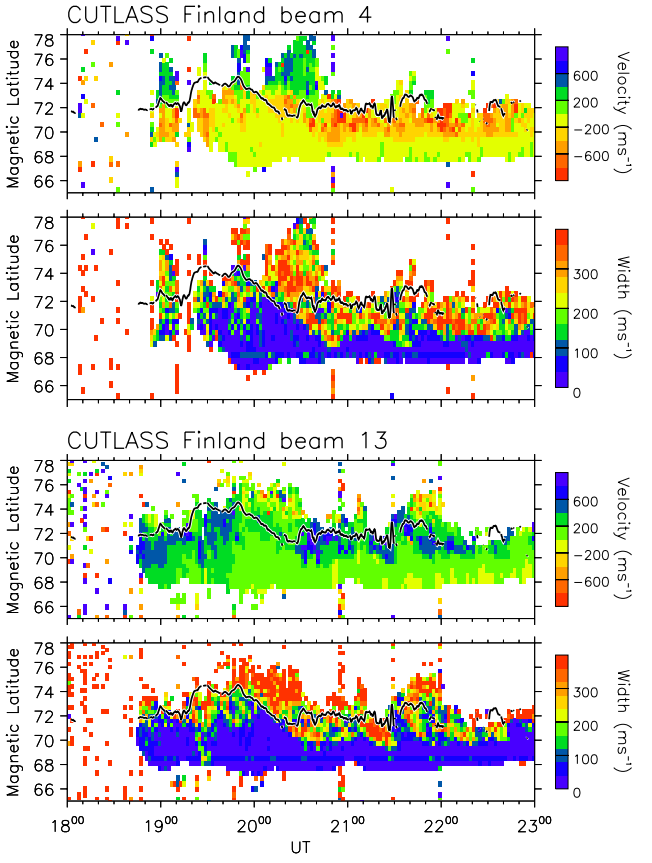

Fig. 5. Line of sight velocity and spectral width for beam 4 (top two panels) and beam 13 (bottom two panels) for the same interval as Fig. 4. The full line marked on each panel of the radar data represents the poleward 1.5 kR contour of the 630.0 nm emission (see text for full discussion).

reaching 71° magnetic latitude at 2300 UT.

Moving to the MSP data we start with the 630.0 nm emission (Fig. 4, panel 4), which is plotted from 0° zenith angle to −90° zenith angle, i.e. from the zenith to the southeast of Svalbard. Between 1800 and 1845 UT the emission is generally fairly weak, with a narrow band of higher intensity emission between 1.0 and 1.5 kR, centred at about −60° zenith angle. At ∼1845 UT, there was a small increase in the intensity of the emission which was coincident with the onset of the radar backscatter. Then at ∼1900 UT, there was a further brightening of the red line emission which lead to an extension of the zenith angle coverage to between −50° and −70°, although still centred at the same latitude. At 1920 UT, there was an enhancement in the emission intensity to greater than 4.5 kR as well as an expansion in extent of the emission region to between −20 and −90° zenith angle. We interpret this as a result of the onset of the substorm expansion phase, identified by the enhanced electrojet observed by the IMAGE magnetometers (see later discussion). By 1930 UT, the emission intensity had started to decrease, although there was another enhancement between 1940 and 1950 UT. Thereafter, the emission intensity declined to the level, location and extent present before 1920 UT. There were further increases in emission intensity near 2040, 2120 and 2140 UT. After this time, there was considerable structure in the red line emission, which, although not increasing in intensity, did increase in extent. After 2200 UT, the red line began to fade again to values less than 1.5 kR.

The green line (557.7 nm) emission (Fig. 4, bottom panel), which is plotted in the same format as the red line emission, exhibited much the same behaviour as the red line emission. The intensity of the emission was stronger, exceeding 9 kR during the intervals of more intense emission, as well as exhibiting a further enhancement in emission intensity after 1950 UT, albeit over a much narrower latitudinal region. Furthermore, just prior to the major enhancement at 1920 UT, there was a narrow region of strong emission near

$-75°$ zenith angle that began at about 1912 UT, which coincided with the loss of radar backscatter on beam 9. Following 2020 UT, there were enhancements in the green line intensity near $-75°$ zenith angle, which exceeded 8 kR and one much weaker enhancement near 2140 UT. Apart from a short interval of relatively weak emission between 2140 and 2200 UT, there was little green line emission after 2125 UT.

Returning to the radar data, in Fig. 5 we present the velocity and spectral width for beams 4 (top two panels) and 13 (bottom two panels) in order to illustrate a number of features. First, by inspection of the velocity data, we note that for most of the interval the velocities measured along beam 4 were negative, away from the radar, with some positive values at the higher latitudes. Along beam 13, the opposite was true, with mainly positive values but also with a few negative values at higher latitudes. These measurements are consistent with a dominant westward (or sunward) flow direction at the lower latitudes and an eastward (or antisunward) flow direction at the higher latitudes. This conclusion has been confirmed by a beam swinging analysis of the radar data. The second feature is that the spectral width behaved in essentially the same way on beams 4 and 13, as it did on beam 9. Indeed, inspection of all the beams demonstrates this behaviour, although the latitude of the boundary does differ slightly from beam to beam. Finally, we note that there was no loss of scatter on beam 13 at about 1912 UT, as on beams 4 and 9. Indeed, the four eastern most beams did not lose scatter at this time.

4 Discussion

To summarise the observations, the interval under discussion is one during which IMF B_z was mainly weakly positive with a negative B_y and $|B_y| > |B_z|$. The solar wind dynamic pressure varied weakly and was typically $\sim$1 nPa. There are three features in the magnetometer, radar and optical data which are of special interest: the substorm-like features observed in the magnetometer and optical data at high latitudes, the boundary in the spectral width, and the equatorward moving bands of spectral width. We begin by discussing the substorm features, before moving to the boundary in the spectral width and finally, the equatorward moving bands of large spectral width.

4.1 High-latitude substorm onset

It is well established that the onset of the expansion phase of a magnetospheric substorm is identified by an auroral signature and a magnetic signature (e.g. Akasofu, 1968). In the Scandinavian sector these signatures normally occur at magnetic latitudes of 65–67°, before a poleward expansion takes place (e.g. Lester et al., 1995; Fox et al., 1999). The main magnetic signature results from an enhanced westward electrojet which is generally co-located with the optical luminosity and thus, enhanced E-region conductivity. At $\sim$1917 UT, there is clear evidence in the magnetometer stations of a weak, but well defined westward electrojet (Fig. 3). The relevant signatures are a negative deflection in the X component and a negative (positive) deflection in the Z component of the stations equatorward (poleward) of the electrojet centre. Such signatures are clearly defined in Fig. 3, between 1917 and 1955 UT, with the electrojet centre occurring near HOR at 73.9° magnetic latitude. At the same time, there was an initial enhancement of the equatorward most auroral arc which was followed by a rapid poleward expansion of the aurora. Close inspection of the 557.7 nm emission data (Fig. 4, bottom panel) indicate that there was an initial enhancement at $\sim$1912 UT of the equatorward most auroral form and a subsequent rapid poleward motion at $\sim$1918 UT. If we assume an altitude of 110 km at which the green line emission maximises, then the latitude of the initial onset is 71° magnetic latitude and the aurora subsequently expands poleward to a maximum latitude of about 74° magnetic latitude. The justification for the altitude of emission is given later in Sect. 4.2.1. Note also that the intensification in the red and green lines at $\sim$1939 UT was accompanied by an intensification of the electrojet, as indicated by the perturbation in the X and Z components of the magnetic field (Fig. 3).

Thus, we have two well defined signatures which suggest a substorm expansion phase onset, albeit at high latitudes and following a period of about 50 minutes when the IMF B_z component had been predominantly northward with a short 10 minute interval of southward IMF. Other signatures generally associated with the onset of the expansion phase include mid latitude Pi2 pulsations and energetic particle injections at geosynchronous orbit. Investigation of the available data sets indicates that neither of these was observed. This does not mean, however, that the signatures reported here are not of a magnetospheric substorm. The latitude of the auroral break up suggests that the geosynchronous signature would not necessarily be expected. A simple mapping of the magnetic field using the T89 model (Tsygenenko, 1990) from 71° magnetic latitude for quiet magnetic conditions ($Kp = 0$) compared with one from 66° magnetic latitude for moderately disturbed conditions ($Kp = 2$) demonstrates this point. In the former case, the field maps to a position $\sim$17 R_E down tail, while in the latter, the field line maps to $\sim$6.6 R_E down tail. If the mapping is correct and the onset did occur at such a large distance in the tail, it seems unlikely that any particle injection signatures would have reached geosynchronous orbit. Often, during the growth phase of magnetospheric substorms, pseudo break-ups occur, which have many of the signatures of the expansion phase onset but which are localised in extent (e.g. Lester et al., 1998). The major difference between the two is that the rapid poleward expansion of the auroral activity, which occurs at expansion phase onset, does not occur at the time of a pseudo break-up. A rapid poleward motion of the aurora did occur during the event under discussion and we conclude that the event is a weak substorm expansion phase occurring at high latitudes following an interval of weak energy storage. Small magnetospheric substorms during intervals of northward IMF B_z have been discussed by a number of authors (e.g. Nishida, 1971; Petrukovich et al.,

2000) and are found to occur on a contracted auroral oval (Akasofu et al., 1973). Craven and Frank (1991), in a study of some 68 expansion phase onsets observed by the imager on DE-1 from a five month interval, found the location of onset varied between 59 and 72° magnetic latitude, with a median value of 65° magnetic latitude. Note that these events had been selected such that the auroral bulge was of limited extent and that there were sufficient images to identify the continuing substorm development. Despite the possibility of selection effects, the study of Craven and Frank does suggest that substorms with onsets at the latitudes of 71° are infrequent.

The onset of the substorm resulted in an initial drop out of radar scatter at 1912 UT which was then followed by a bite out of scatter at about 1922 UT, after the scatter had returned at 1917 UT. This behaviour has been reported before by Yeoman et al. (2000), who suggested that the initial drop out of scatter is caused by the brightening of the arc which results in the flow stagnating poleward of the arc. This stagnation results in the electric field going to zero, which, in turn, leads to the disappearance of the backscatter (Milan et al., 1999). The scatter then returns after the flow has re-oriented such that it avoids the obstacle of the high conductivity region associated with the brightening of the auroral arc. The resulting bite out in the scatter is then associated with the poleward expansion of the auroral activity. Some of the HF signals, probably the high angle rays, are absorbed by the enhanced E-region and possibly D-region electron densities associated with this larger region of auroral activity (Yeoman et al., 2000).

4.2 High spectral width boundary

We move now to discuss the boundary in the spectral width observations and, in particular, the cause of the large spectral widths at the high latitude part of the field of view, and whether the boundary is of geophysical significance in relation to a magnetospheric boundary. Large spectral widths in HF radar backscatter were first discussed in association with the footprint of the ionospheric cusp (Baker et al., 1990, 1995). No specific reason for the large spectral width was given at the time, although Baker et al. (1995) did suggest that the spectra resulted from a variety of both temporal and spatial behaviour within the cusp region. Certainly there was evidence from coincident DMSP passes that both variable electric fields and particle precipitation were present in range gates where the spectra were large. Subsequent observations of large spectral width on the nightside were reported by Lewis et al., 1997 and Dudeney et al., 1998. In the example discussed by Dudeney et al. (1998), the boundary between small and large spectral width was seen to straddle the boundary between the central plasma sheet (CPS) and the boundary plasma sheet (BPS). Thus, the large spectral width region was related to the boundary plasma sheet. More recently, however, André et al. (1999, 2000) have suggested an alternative cause for the large spectral width associated with the cusp. These authors propose that the spectral width is a result of the electric fields associated with ULF wave activity in the cusp area modifying the spectra, or more exactly, the radar autocorrelation function.

4.2.1 Polar cap boundary definition

It has been suggested that the poleward border of the red line emission is co-located with the polar cap boundary, i.e. the boundary between open and closed magnetic flux (Samson et al., 1992; Blanchard et al., 1995). Samson et al. (1992) identified the poleward border of the red line emission with the equatorward boundary of the polar rain based upon simultaneous DMSP electron measurements, which they assume to be the boundary between open and closed field lines. Blanchard et al. (1995) looked at this suggestion in some detail and concluded that the red line emission could be used as a good monitor for the polar cap boundary. It is clear from their measurements, however, that there are several times when the co-location is not as good as their suggested precision of $\pm 0.9°$ invariant latitude. This is particularly the case when the nightside auroral oval is dynamic, e.g. during the expansion phase of a substorm, suggesting therefore, that under these conditions, the red line emission is not a good proxy for the polar cap boundary.

In order to undertake a direct comparison between the spectral width and the MSP data, the latter needs to be transformed into magnetic latitude co-ordinates. This is not, however, a trivial task, as the optical emission can come from a range of altitudes and therefore, assuming a single altitude of emission is not always correct. The red line emission is particularly difficult as it can come from altitudes between 200 and 500 km, with the altitude of the peak emission normally expected to be near 250 km. The green line emission comes from a much narrower height range, ∼100–120 km, with the peak emission at ∼110 km. Careful investigation of the optical data, including all sky camera data not shown, indicates that there were two discrete, narrow, ∼10 km wide, auroral features equatorward of Longyearbyen for most of the interval, although not during the substorm expansion phase. For certain times the latitude of the lower border of the poleward most auroral form can be compared with the latitude of the poleward border of the red line, assuming a uniform height of 250 km for the emission. At these times, the difference between the two latitudes is a fraction of a degree, which is of the order of the length of a radar range gate, 45 km. As the difference is small for certain times, we have calculated the poleward boundary of the red line emission assuming a uniform altitude of emission of 250 km. Assuming then an altitude of emission for the green line of 110 km, there is excellent agreement in the latitudes of the red and green line emissions, which further supports the general use during this interval of the single altitude of emission for the red line.

The poleward border is, in fact, the 1.5 kR contour and this has been overlaid on the radar data in Figs. 4 and 5. This contour is well defined and inspection of the data indicates that the gradient of the emission intensity is such that the actual value employed is not important. The location of the contour was close to 72° magnetic latitude between 1845 and

1920 UT before jumping poleward to 74° magnetic latitude at the time of the enhancement in emission. Thereafter, the contour remained between 73 and 74° magnetic latitude until 1950 UT, whereupon it moved steadily equatorward over the next 30–40 minutes, reaching 71° magnetic latitude. Another poleward jump to just over 72° magnetic latitude took place at about 2030 UT after which, this contour remained approximately at the same latitude until 2115 UT. This was followed by a short interval when the contour varied somewhat before a poleward jump to 73° magnetic latitude at 2135 UT, where it remained for 15 minutes before moving equatorward to 71° magnetic latitude at 2200 UT. After 2200 UT, the red line emission was in general less than 1.5 kR.

4.2.2 Polar cap boundary and spectral width

Comparing the 1.5 kR contour with the spectral width data in the central panel of Fig. 4, we see that at the start of the interval the 1.5 kR contour and the boundary between large and small spectral widths agreed to within one degree for the first 12 minutes. After the scatter returned at 1920 UT, the two boundaries did not agree. When the 1.5 kR contour began to move equatorward at about 2000 UT, however, there was, in general, good agreement between the two boundaries, until the second poleward jump of the 1.5 kR contour at 2030 UT. Thereafter, there was again a discrepancy between the latitude of the poleward border of the red line and that of the gradient in the spectral width. Close inspection of the spectral width data suggests that the difference was caused by equatorward moving bands of large spectral width, such that there were regions of smaller spectral width just equatorward of the 1.5 kR contour. The highest latitude of these regions of small spectral width does appear to agree reasonably well with the 1.5 kR contour.

The location of the poleward border of the red line emission was quantified by Blanchard et al. (1995) by fitting a step function in latitude to the emission measurements, assuming approximately constant emission levels in the polar cap and in the auroral oval. Although this method differs somewhat from the simple use of the 1.5 kR contour, careful investigation of the emission profile with latitude indicates that both methods result in similar locations for the interval discussed here. In addition, Fig. 4 demonstrates that the emission intensity was not constant with latitude within the auroral oval. We can extend the analysis discussed earlier by considering the occurrence frequency of spectral width poleward and equatorward of the 1.5 kR contour. Figure 6 presents the occurrence distribution for these two regions of scatter in bins of 50 m s^{-1}, poleward of the 1.5 kR contour in the top panel and equatorward of the contour in the bottom panel. Note that in the bottom panel, the distribution poleward of the contour is overlaid (Fig. 6, lower panel, thin line). The distributions are calculated for the interval 1845–2300 UT and if the poleward 1.5 kR contour in the red line emission was not present, the radar data would not have been included. The boundary is assumed to have been at a constant latitude over the whole radar field of view in order that

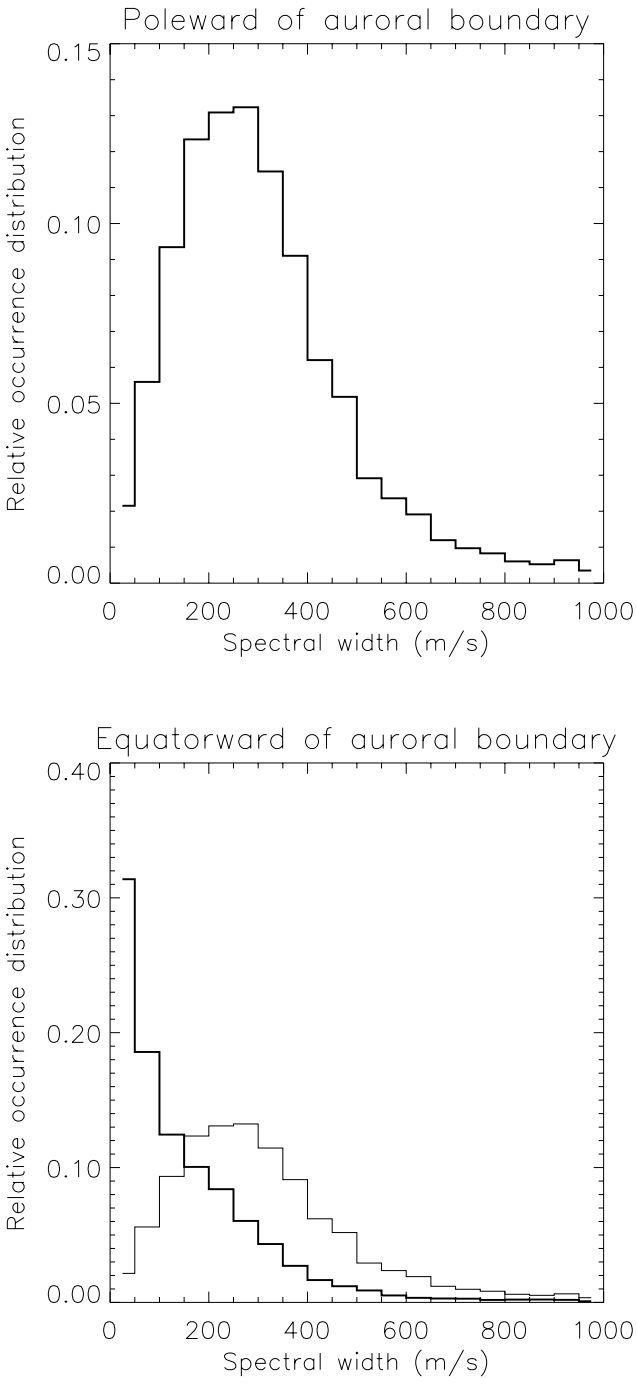

Fig. 6. Occurrence histograms of spectral width poleward of the 1.5 kR contour (upper panel) and equatorward of the 1.5 kR contour (lower panel, thick line). Note the distribution from the upper panel is overlaid in the lower panel as a thin line.

we can include data from all 16 beams. The distribution of spectral width poleward of the 1.5 kR contour (Fig. 6, upper panel) peaks in the 250–300 m s^{-1} bin, at 13% of the distribution. If we consider 200 m s^{-1} as representative of the boundary between small and large spectral widths, we find that 70% of the distribution had spectral widths > 200 m s^{-1}. The occurrence distribution of spectral width equa-

torward of the 1.5 kR contour (Fig. 6, lower panel, thick line) is very different. The peak spectral width occurrence frequency is between 0 and 50 m s^{-1}, with 31% of the distribution; 72% of the distribution had a spectral width which is < 200 m s^{-1}. These distributions indicate that there was a significant relationship between the 1.5 kR contour and the spectral width parameter. Note that the two distributions in Fig. 6 do not change shape if a different time interval or contour of red line intensity is chosen. The percentages above and below the threshold value of 200 m s^{-1} do change, but overall, $\sim$70% of each distribution is larger or smaller than 200 m s^{-1} poleward or equatorward of the 1.5 kR contour, respectively.

4.2.3 Polar cap boundary and flow reversal boundary

Comparison with the radar line of sight velocity measurements can also be made. However, beam 9 is not ideal to undertake such a comparison as it points almost along a magnetic meridian and hence, the velocity measurements will, in general, be small if the flow is primarily eastwards or westwards. Therefore, we undertake the same process with two beams, 4 and 13, which point to the west and east of beam 9, respectively, and are, therefore, at an angle to the meridian. The line of sight velocity and spectral width measurements for beam 4 (top two panels) and beam 12 (bottom two panels) are given in Fig. 5. If we consider the velocity measurements along beam 4 first, we note that initially the 1.5 kR contour was coincident with a boundary between positive velocities in the poleward part of the scatter region and negative velocities in the equatorward part of the scatter region, which is equivalent to the FRB. When backscatter returned at 1920 UT, there was limited scatter poleward of the 1.5 kR contour, but equatorward of this, all velocities were negative. Between 1945 and 1955 UT, the 1.5 kR contour is close to the same latitude as the boundary between positive and negative velocities, although the two boundaries are moving in different directions and can differ by 2 degrees of magnetic latitude. From 2005 UT until 2025 UT, however, there were positive velocities poleward of the 1.5 kR contour as this contour moved equatorward. After 2025 UT, there was a brief period when the two boundaries were again in close agreement and from 2045 UT onwards there was little scatter poleward of the 1.5 kR contour; all velocities equatorward of this contour were negative. Comparison with the spectral width measurements on beam 4 (Fig. 5, second panel) indicates similar results to those discussed for beam 9. The separation of two regions of large spectral width by a region of small spectral width after 2020 UT, as a result of the equatorward moving bands of high spectral width, is confirmed with this particular beam. Moving to the beam 13 measurements (Fig. 5, bottom two panels), equatorward of the 1.5 kR contour the line of sight velocity was predominantly positive, while the only negative velocity measurements were poleward of this contour between 1940 and 2030 UT, near 2110 UT and between 2140 and 2200 UT. The spectral width measurements, however, do demonstrate a well defined boundary which behaved very similarly to that in beams 4 and 9. Finally, we note that coincident with the intervals of equatorward moving regions of large spectral widths, there were regions of larger line of sight velocities, positive in beam 13 and negative in beam 4. These larger line of sight velocities occurred within a narrow region of typically 1–2° of magnetic latitude.

4.2.4 High spectral width and particle precipitation

Before discussing the relationship between the red line emission and the spectral width and flow reversal boundary, we need to assess the relationship between the red line emission and the polar cap boundary. In terms of electron precipitation signatures, the boundary between open and closed field lines can be considered to be equivalent to the boundary between the polar rain and precipitation from the boundary plasma sheet. The polar rain is characterised by a weak electron flux with an average energy of 100 eV (Hardy et al., 1986), while precipitation associated with the plasma sheet is characterised by more intense and more energetic electron precipitation (Winningham et al., 1975). The exact mapping between the auroral oval and the boundary plasma sheet is subject to continuing debate (e.g. Galperin and Feldstein, 1991). This debate, however, need not concern us here as we are only interested in the poleward boundary of the auroral oval, which we associate with the polar cap boundary or the boundary between open and closed field lines. The red line emission in the nightside auroral oval is generally believed to result from precipitating electrons of energies ≤ 1 keV. This is due to a combination of the effect of the long lifetime of the singlet D upper state and the cross section for excitation. Given the average energies and particle fluxes, it is, therefore, reasonable to assume that the red line emission would map to boundary plasma sheet rather than polar rain, i.e. closed magnetic field lines.

The latitudinal gradient in the spectral width on the nightside has been discussed before (Lewis et al., 1997; Dudeney et al., 1998). In these two studies the gradient in the spectral width appeared to straddle the boundary between the central plasma sheet and the boundary plasma sheet. In the study by Dudeney et al. (1998), a comparison of radar spectra was made with coincident data from the Polar Hydra instrument which measures electrons and ions in the 20 eV to 10 keV energy range. Lewis et al. (1997) noted that the region of scatter, within which there was a gradient in spectral width, corresponded to a region of magnetospheric precipitation near the boundary plasma sheet and central plasma sheet. The DMSP spacecraft provides an excellent data set of particle measurements from which estimates of the poleward boundary of the oval can be made (e.g. Hardy et al., 1986). While there are no DMSP passes through the radar field of view during the interval of radar scatter, one spacecraft passed through, just prior to the interval of scatter. The ion and electron spectrograms in the energy range 20 eV to 30 keV measured by F12 are given in Fig. 7. These data are taken from a pass through the radar field of view between $\sim$1841 and 1846 UT, just prior to the onset of radar

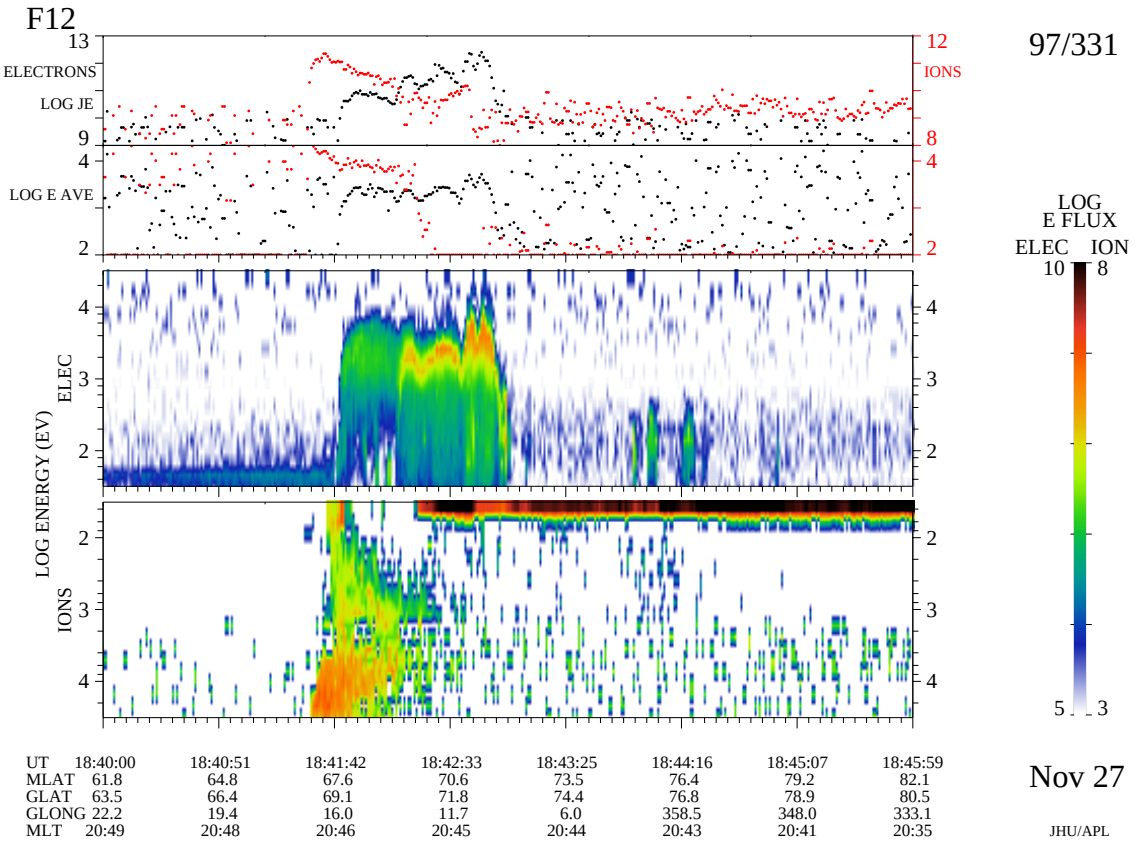

Fig. 7. Spectrograms of electrons and ions (lower two panels) in the 20 eV to 20 keV energy range for the interval 1840–1846 UT from the DMSP F12 spacecraft.

backscatter and when both red and green line emissions were relatively weak. The pass is used to demonstrate the nature of the precipitation within the oval and how the boundary may be determined. The spacecraft, moving polewards, encountered ion precipitation with average energy ∼30 keV at 1841:30 UT before the electron precipitation of average energy 1–5 keV at 1841:45 UT. The ion precipitation gradually decreased in energy as F12 moved poleward until ∼1842:25 UT when the ion precipitation ceased. The electron flux increased by an order of magnitude at ∼1842:12 UT, and thereafter, although varying gradually increased until ∼1842:53 UT when there was a rapid drop in both flux and average energy. This rapid decrease has been identified as the poleward boundary of the main auroral oval (Newell et al., 1996). The spacecraft finally exited the electron precipitation at 1843:04 UT, which is the poleward boundary of the subvisual drizzle, which differs from polar rain (Newell et al., 1996). Note that as well as the increasing flux, the average energy of the electrons peaked at ∼ 4–6 keV prior to 1842:51 UT.

Based upon these times and converting the geographic coordinates to altitude adjusted corrected geomagnetic coordinates, AACGM, (Baker and Wing, 1989), we note that the initial drop in electron flux and average energy at ∼1842:53 UT occurred at 71.6° magnetic latitude, while the final reduction in electron flux occurred at 71.9° magnetic latitude. At the start of the radar backscatter, ∼1848 UT, the poleward border of the red line emission was ∼71.9° magnetic latitude, while the boundary in the spectral width was at ∼72.6° magnetic latitude.

Based upon the observations of radar spectral width discussed above, the high spectral width region mapped to polar rain type precipitation while the low spectral width region mapped to plasma sheet precipitation. Here, we do not distinguish between central plasma sheet or boundary plasma sheet. The low spectral width region is associated with the auroral emission in both red and green lines, which occur at different altitudes. In general, the behaviour of the green line was similar to the red line. Therefore, the low spectral width mapped to the region where the ionospheric electron density distribution was most likely to be more structured due to particle precipitation.

In summary, on average, low spectral widths were associated with the auroral luminosity in both the red and green lines and precipitation with average energy of a few keV. The large spectral widths, however, were associated with low auroral luminosity and precipitation characteristic of the polar cap, i.e. polar rain. Furthermore, the motion of the poleward border of the red line with time mirrored the motion of the gradient in the spectral width. Based on these observations, we conclude that particle precipitation associated with

the auroral luminosity is not the cause of the large spectral width. This disagrees with the previous reported observations of the gradient in spectral width (Lewis et al., 1997; Dudeney et al., 1998). There were, however, three intervals when the collocation of the poleward border of the auroral luminosity and the gradient in the spectral width broke down: during the substorm, during the equatorward moving bands, and after 2200 UT when the luminosity went to low levels.

4.3 Equatorward moving bands

We finish the discussion with a further investigation of the equatorward moving bands. Figure 8 presents the line of sight velocity (top panels) and the spectral width (lower panels) for two consecutive scans starting at 2032 UT and 2034 UT. The data are plotted in magnetic local time-magnetic latitude coordinates. Magnetic midnight is at the bottom of each panel. Overlaid on each panel is the statistical Feldstein oval for $Kp = 0$ (Feldstein and Starkov, 1967; Holzworth and Meng, 1975). We see that there was a narrow region of large spectral width embedded within a region of low spectral width. This narrow region of large spectral width was approximately aligned with the poleward border of the statistical oval. Also aligned along this border was a narrow channel of high flow velocities, negative in the west and positive in the east, and thus, consistent with an overall westward flow at that time.

Equatorward moving arcs on the nightside are a common phenomenon during the growth phase and even early expansion phase of magnetospheric substorms (Persson et al., 1994; Gazey et al., 1995). Similar features in the ion velocity have been reported by Lester et al. (1995) in the early expansion phase. However, there is no indication of any substorm activity during or following these observations. Other intensifications at the poleward edge of the auroral oval during quiet intervals have been discussed by de la Beaujardière et al. (1994). In this study intensifications of the poleward most arc were found to occur every 10–20 minutes associated with the formation of a new arc poleward of the former. Furthermore, once every hour or so, stronger intensifications occurred which drifted equatorward at $\sim$270 m s^{-1}. The local plasma velocity doubled in value and a reversal in the east-west component formed. This disturbance moved westward at 900 m s^{-1} through the Sondrestrom and Goose Bay radar fields of view. In one instance, a simultaneous observation of a velocity dispersed ion signature at a low altitude spacecraft was observed. The conclusion reached by de la Beaujardiere et al. was that these features were related to a local increase in the reconnection rate in the tail. These observations are in agreement with predictions of the so-called expanding contracting polar cap model for the generation of ionospheric flows (Cowley and Lockwood, 1992).

Comparing the observations reported here throughout the interval of equatorward moving bands, the IMF B_z component varied between 0 and 2 nT, while B_y was -5 nT apart from a brief 15 minute interval when B_z was $+5$ nT and B_y -1 nT. During the interval reported by de la Beaujardiére

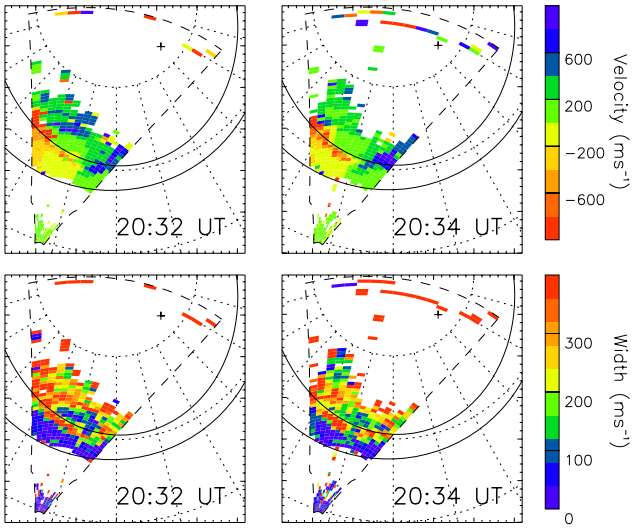

Fig. 8. Full radar scans of line of sight velocity (top panels) and spectral width (bottom two panels) for scans starting at 2032 UT and 2034 UT. The coordinate system is magnetic local time/magnetic latitude based upon the AAGCM coordinates of Baker and Wing (1989).

et al. (1994), however, the B_x component was the dominant IMF component which is not the case in the interval discussed here. We note a number of similarities between the two intervals, e.g. the generally quiet global magnetic conditions, the equatorward drift, the repetition rate and the channel of enhanced westward flow. We note, also, that there were regions of strong equatorward flow embedded within the weaker flow poleward of the FRB in both radar scans presented in Fig. 8. In the first, there was a region in the centre of the field of view, near 23 MLT and 75° magnetic latitude, as well as one in the eastern part of the field of view near 24 MLT and 72° magnetic latitude. The former lasted for only one scan, while the latter was present for a longer time period. Such features are consistent with the observations of de la Beaujardiére et al. (1994) who also noted enhanced equatorward flow. If the poleward border of the red line emission does represent the polar cap boundary, then this is the ionospheric footprint of the last closed field line in the tail. Hence, this is the most likely site for reconnection at the distant neutral line to be taking place.

5 Conclusions

In summary, we find that in this particular case study there is evidence that a gradient in spectral width is related to the PCB, with large spectral widths co-located with polar rain electron precipitation poleward of the PCB. As the particle precipitation associated with the large spectral widths is of polar rain levels, it is unlikely that structured electron precipitation plays a role in the formation of these large spectral widths, as proposed by Lewis et al. (1997) and Dudeney et al. (1998). In this case, therefore, some alternative explana-

tion of the large spectral widths is needed. It is likely that the recent work of André et al. (1999, 2000) will provide such an explanation.

The relationship between the spectral width gradient and the auroral luminosity was, however, complicated by dynamical features. The first was a magnetospheric substorm which occurred at higher than usual magnetic latitudes. The second was related to equatorward moving bands of large spectral width. The substorm occurred immediately following an interval of weak energy input to the magnetosphere, as characterised by the IMF and solar wind conditions, although weak this event does indicate that such bursts of activity can occur during such solar wind conditions. The equatorward moving bands are also intriguing and we conclude that they may have been caused by time dependent reconnection at a distant neutral line following the substorm onset. This study illustrates the complexity of the polar cap during quiet conditions. There was evidence for both substorm activity and continued bursts of reconnection at the polar cap boundary. The magnetosphere ionosphere system does not remain stable under such weakly northward IMF conditions.

We conclude finally that the gradient in the spectral width may be used as a proxy for the PCB, but only with extreme care. Dynamical features can clearly cause some difficulty and further work needs to be done to establish the detailed relationship between the spectral width and the PCB.

Acknowledgements. The authors would like to thank the CUTLASS team for their continued efforts to maintain the CUTLASS system supported by PPARC grant PPA/R/R/1997/00256. The DMSP series SSJ/4 particle detectors were designed and built by Dave Hardy and colleagues at Phillips Laboratory. The DMSP spectrogram was provided by the Applied Physics Laboratory, Johns Hopkins University. Funding for placing this spectrogram data online was provided by NASA grant No. NAG5-7189 to Simon Wing. SEM is supported on grant PPA/G/O/1999/00181.

The Editor in chief thanks P. E. Sandholt and R. Andre for their help in evaluating this paper.

References

Akasofu, S.-I., Polar and magnetospheric substorms, D. Reidel Publ. Co., Dordrecht, 1968.

Akasofu, S.-I., Perreault, P. D., Yasuhara, F., and Meng, C.-I., Auroral substorms and the interplanetary magnetic field, J. Geophys. Res., 78, 7490–7508, 1973.

André, R., Pinnock, M., and Rodger, A. S., On the SuperDARN autocorrelation function observed in the ionospheric cusp, Geophys. Res. Lett., 26, 3353–3356, 1999.

André, R., Pinnock, M., and Rodger, A. S., Identification of the low-altitude cusp by Super Dual Auroral Radar Network radars: A physical explanation for the empirically derived signature, J. Geophys. Res., 105, 27081–27093, 2000.

Baker, K. B. and Wing, S., A new magnetic co-ordinate system for conjugate studies at high latitude, J. Geophys. Res., 94, 9139–9143, 1989.

Baker, K. B., Greenwald, R. A., Ruohoniemi, J. M., Dudeney, J. R., Pinnock, M., Newell, P. T., Greenspan, M. E., and Meng, C.-I., Simultaneous HF-radar and DMSP observations of the cusp, Geophys. Res. Lett., 17, 1869–1872, 1990.

Baker, K. B., Dudeney, J. R., Greenwald, R. A., Pinnock, M., Newell, P. T., Rodger, A. S., Mattin, N., and Meng, C.-I., HF radar signatures of the cusp and low latitude boundary layer, J. Geophys. Res., 100, 7671–7695, 1995.

Blanchard, G. T., Lyons, L. R., Samson, J. C. and Rich, F. J., Locating the polar cap boundary from observations of 6300 Å auroral emission, J. Geophys. Res., 100, 7855–7862, 1995.

Brittnacher, M. Filligam„ M., Parks, G., Germany, G., and Spann, J., Polar cap area and boundary motion during substorms, J. Geophys. Res., 104, 12251–12262, 1999.

Cowley, S. W. H., Excitation of flow in the Earth's magnetosphere-ionosphere system: Observations by incoherent-scatter radar, in Polar Cap Boundary Phenomena, Eds. J. Moen et al., pp 127–140, Kluwer Academic Publishers, Netherlands, 1998.

Cowley, S. W. H. and Lockwood, M., Excitation and decay of solar wind-driven flows in the magnetosphere-ionosphere system, Ann. Geophysicae, 10, 103–115, 1992.

Craven, J. D. and Frank, L. A., Diagnosis of auroral dynamics using global aurora imaging with emphasis on large-scale fluctuations, in Auroral Physics, Eds. C.-I. Meng et al., pp 273–288, Cambridge University Press, Cambridge, 1991.

de la Beaujardiere, O., Lyons, L. R., Ruohoniemi, J. M., Friis-Christensen, E., Danielsen, C., Rich, F. J., and Newell, P. T., Quiet-time intensifications along the poleward auroral boundary near midnight, J. Geophys. Res., 99, 287–298, 1994.

Dudeney, J. R., Rodger, A. S., Freeman, M. P., Pickett, J., Scudder, J., Sofko, G., and Lester, M., The nightside ionospheric response to IMF B_y changes, Geophys. Res. Lett., 25, 2601–2604, 1998.

Feldstein, Y. I. and Starkov, G. V., Dynamics of auroral belt and polar geomagnetic disturbances, Planet. Space Sci., 15, 209–230, 1967.

Fox, N. J., Cowley, S. W. H., Davda, V. N., Enno, G., Friis-Christensen, E., Greenwald, R. A., Hairston, M. R., Lester, M., Lockwood, M., Lühr, H., Milling, D. K., Murphree, J. S., Pinnock, M., and Reeves, G. D., A multipont study of a substorm occurring on 7 December 1992 and its theoretical implications, Ann. Geophysicae, 17, 1369–1384, 1999.

Galperin, Yu. I. and. Feldstein, Ya. I, Auroral luminosity and its relationship to magnetospheric plasma domains, in Auroral Physics, Eds. C.-I. Meng et al., pp 207–222, Cambridge University Press, Cambridge, 1991.

Gazey, N. G. J., Lockwood, M., Smith, P. N., Coles, S., Bunting, R. J., Lester, M., Aylward, A. D., Yeoman, T. K., and Lühr, H., Development of substorm cross-tail current disruption as seen from the ground, J. Geophys. Res., 100, 9633–9648, 1995.

Greenwald, R. A., Baker, K. B., Dudeney, J. R., Pinnock, M., Jones, T. B., Thomas, E. C., Villain, J.-P., Cerisier, J.-C., Senior, C., Hanuise, C., Hunsucker, R. D., Sofko, G., Koehler, J., Nielsen, E., Pellinen, R., Walker, A. D. M., Sato, N., and Yamagishi, H., Darn/Superdarn: A global view of the dynamics of high-latitude convection, Space Sci. Rev., 71, 761–796, 1995.

Hardy, D. A., Gussenhoven, M. S., Riehl, K., Burkhardt, R., Heinemann, N., and Schumaker, T., The characteristics of polar cap precipitation and their dependence on the interplanetary magnetic field and the solar wind, in Solar Wind-Magnetosphere Coupling, Eds. Y. Kamide and J. A. Slavin, pp 575–604, Terra Sci. Pub. Co., Tokyo, 1986.

Holzworth, R. H. and Meng, C.-I., Mathematical representation of the auroral oval, Geophys. Res. Lett., 2, 377–380, 1975.

Kamide, Y. and Kokubun, S., Two-component auroral electrojet:

Importance for substorm studies, J. Geophys. Res., 101, 13027–14046, 1996.

Lepping, R. P., Acuna, M. H., Burlaga, L. F., Farrell, W. M., Slavin, J. A., Schatten, K. H., Mariani, F., Ness, N. F., Neubauer, F. M., Whang, Y. C., Byrnes, J. B., Kennon, R. S., Panetta, P. V., Scheifele, J., and Worley, E. M., The Wind magnetic field investigation, Space Sci. Rev., 71, 207–229, 1995.

Lester, M., HF coherent scatter radar observations of ionospheric convection during magnetospheric substorms, Adv. Polar Upper Atmos. Res., 14, 179–201, 2000.

Lester, M., Freeman, M. P., Southwood, D. J., Waldock, J. A., and Singer, H. J., A study of the relationship between interplanetary parameters and large displacements of the nightside polar cap, J. Geophys. Res., 95, 21133–21145, 1990.

Lester M., Lockwood, M., Yeoman, T. K., Cowley, S. W. H., Lühr, H., Bunting, R., and Farrugia, C. J., The response of ionospheric convection in the polar cap to substorm activity, Ann. Geophysicae, 13, 147–158, 1995.

Lester, M., Jones, T. B., Robinson, T. R., Thomas, E. C., Yeoman, T. K., Pellinen, R., Huuskonen, A., Opgenoorth, H., Persson, M., Pellinen-Wannberg, A., and Haggstrom, I., CUTLASS – A tool for co-ordinated space/ground based investigations of the solar terrestrial system, in Satellite – Ground Based Coordination Sourcebook, ESA-SP-1198, 191–202, Eds. M. Lockwood, M. N. Wild and H. J. Opgenoorth, ESA Publications, ESTEC, Noordwijk, The Netherlands, 1997.

Lester, M., Milan, S. E., Baker, K., Greenwald, R. A., Brittnacher, M., Lummerzheim, D., Owen, D., Pulkinnen, T., Reeves, G. D., Sofko, G., and Villain, J.-P., Polar, IMP-8 and SuperDARN observations of substorm growth and expansion phase signatures, SUBSTORMS-4 (Eds. S. Kokubun and Y. Kamide), 175–178, Terra Scientific Publishing Corporation, 1998.

Lewis, R. V., Freeman, M. P., Rodger, A. S., Reeves, G. D., and Milling, D. K., The electric field response to the growth phase and expansion phase onset of a small isolated substorm, Ann. Geophysicae, 15, 289–299, 1997.

Lockwood, M., Cowley, S. W. H., Todd, H., Willis, D. M., and Clauer, C. R., Ion flows and heating at a contracting polar cap boundary, Planet. Space Sci., 36, 1229–1253, 1988.

Milan, S. E., Davies, J. A., and Lester, M., Coherent HF radar backscatter characteristics associated with auroral forms identified by incoherent radar techniques, J. Geophys. Res., 104, 22591–22603, 1999.

Newell, P. T., Feldstein, Y. I., Galperin, Y. I., and Meng, C.-I., Morphology of nightside precipitation, J. Geophys. Res., 101, 10737–10748, 1996.

Nishida, A., Interplanetary origin of electric fields in the magnetosphere, Cosmic Electrodyn., 2, 350, 1971.

Ogilvie, K. W., Chornay, D. J., Fritzenreiter, R. J., Hunsaker, F., Keller, J., Lobell, J., Miller, G., Scudder, J. D., Sittler Jr., E. C., Torbert, R. B., Bodet, D., Needell, G., Lazarus, A. J., Steinberg, J. T., Tappan, J. H., Mavretic, A., and Gergin, E., SWE, A comprehensive plasma instrument for the Wind spacecraft, Space Sci. Rev., 71, 55–77, 1995.

Persson, M. A. L., Aikio, A. T., and Opgenoorth, H., Satellite-groundbased coordination: late growth and early expansion phase of a substorm, in Proc. Second Internat. Conf. on Substorms, Geophys. Institute, Fairbanks, Alaska, pp 157, 1994.

Petrukovich, A. A., Baumjohann, W., Nakamura, R., Mukai, T., and Troshichev, O. A., Small substorms: Solar wind input and magnetotail dynamics, J. Geophys. Res., 105, 21109–21118, 2000.

Reiff, P. H. and Burch, J. L., IMF B_y-dependent plasma flow and Birkeland currents in the dayside magnetopshere. 2. A global model for northward and southward IMF, J. Geophys. Res., 90, 1595–1609, 1985.

Ruohoniemi, J. M. and Baker, K. B., Large-scale imaging of high-latitude convection with Super Dual Auroral radar Network HF radar observations, J. Geophys. Res., 103, 20797–20806, 1998.

Samson, J. C., Lyons, L. R., Xu, B., Creutzberg, F., and Newell, P., Proton aurora and substorm intensifications, Geophys. Res. Letts., 19, 2167–2170, 1992.

Taylor, J. R., Yeoman, T. K., Lester, M., Emery, B. A., and Knipp, D. J., Variations in the polar cap area during intervals of substorm activity on 20–21 March 1990 deduced from AMIE convection patterns, Ann. Geophysicae, 14, 879–887, 1996.

Tsyganenko, N. A., Quantitative models of the magnetospheric magnetic field: methods and results, Space Sci. Rev., 54, 75–104, 1990.

Viljanen, A. and Häkkinen, L., IMAGE magnetometer network, in Satellite – Ground Based Coordination Sourcebook, ESA-SP-1198, 111–118, Eds. M. Lockwood, M. N. Wild and H. J. Opgenoorth, ESA Publications, ESTEC, Noordwijk, The Netherlands, 1997.

Winningham, J. D., Yashura, F., Akasofu, S.-I., and Heikkila, W., The latitudinal morphology of 10-eV to 10-keV electron fluxes during magnetically quiet and disturbed times in the 2100–0300 MLT sector, J. Geophys. Res., 80, 3148–3160, 1975.

Yeoman, T. K., Davies, J. A., Wade, N. M., Provan, G., and Milan, S. E., Combined CUTLASS, EISCAT and ESR observations of an isolated substorm, Ann. Geophysicae, 18, 1073–1087, 2000.